Electronic transport properties of amorphous Ti-Ni and Hf-Ni alloys

1993 J. Phys.: Condens. Matter 5 7251

(http://iopscience.iop.org/0953-8984/5/39/012)

J. Phys.: Condens. Matter 5 (1993) 7251–7258. Printed in the UK

Electronic transport properties of amorphous Ti–Ni and Hf–Ni alloys

K D D Rathnayaka, K Rhie, B D Hennings† and D G Naugle
Department of Physics, Texas A&M University, College Station, TX 77843-4242, USA

Received 15 June 1993

Abstract. Measurements of electrical resistivity ρ and the Hall coefficient R_H of codeposited amorphous $Ti_{1-x}Ni_x$ films from 1.7 K to 300 K over the composition range $0.08 < x < 0.72$ along with measurements of the Hall coefficient for four compositions of melt-spun amorphous $Hf_{1-x}Ni_x$ ribbons are reported. R_H changes sign from positive to negative as the Ni concentration is increased and has a weak temperature dependence. The Hall resistivity of Ni-rich alloys indicates a ferromagnetic transition. For Ni-based amorphous alloys, the critical concentration of Ni at which the Hall coefficient changes sign from positive to negative does not vary appreciably for ETM components of the same column. The room-temperature resistivity ranges from 190 to 300 $\mu\Omega$ cm and shows a small temperature dependence with a negative TCR, which is typical of amorphous alloys. $R_H - R_H^0$ (the Lorentz contribution) shows an almost universal scaling with ρ^2 as a function of Ni composition x for M (Hf, Zr, Ti)–Ni alloys.

1. Introduction

The electronic transport properties of amorphous metal alloys have been extensively studied in the last two decades. One of the most interesting properties of these alloys is the occurrence of a positive Hall coefficient when the alloy is dominated by an early-transition-metal (ETM) component (see reviews by Mizutani [1], Naugle [2], Howson and Gallagher [3] and Naugle and Rhie [4]). Zr-based amorphous alloys constitute one of the most completely studied ETM–LTM (late-transition-metal) alloy systems, where one could see the behaviour of R_H for different LTM components of the same row of the periodic table (Zr–Cu [5, 6], Zr–Ni [7–9], Zr–Co [8, 10], Zr–Fe [8, 11]). As the LTM concentration x is increased, R_H changes sign from positive to negative at a critical concentration x_c, and the value of x_c increases with the LTM column.

Although Ni is the TM component most commonly used [3] in making amorphous alloys, Hall effect data are available only for a limited number of alloy systems and usually only for limited alloy compositions, except for the Ni–Zr system where Hall data are available in a wide composition range [7–9]. Gallagher *et al* [5] have reported the Hall coefficient for several Cu-based amorphous alloys with different ETM components for the same column (Ti, Zr, Hf), but the data are available only for limited compositions. Buschow reported the resistivity [12] and the crystallization temperature [13] for a series of $Ti_{1-x}Ni_x$ amorphous alloys in the composition range $0.23 \leqslant x \leqslant 0.64$. Recently, Lindqvist *et al* [14] reported the Hall coefficient for a few Ni–Ti alloy compositions. In an effort to investigate the influence of the ETM row on the properties of amorphous ETM–LTM alloys we report transport measurements for Ti–Ni and Hf–Ni alloys.

† Current address: NAVSEA 08, James K Polk Building (NC2), 2521 Jefferson Davis Highway, Arlington, VA 22202, USA.

0953-8984/93/397251+08$07.50

2. Experimental methods

Amorphous Ti–Ni films were codeposited onto liquid-nitrogen-cooled fused quartz substrates from two e-beam guns in an ultra-high vacuum (UHV) chamber. The e-beam guns were independently monitored and controlled using two Inficon electron impact emission spectrometry rate monitors to obtain the desired composition. Both source materials were 99.99% pure elements from Johnson Matthey AESAR company. The base pressure of the system was in the low 10^{-10} Torr range and the deposition pressure was approximately 10^{-9} Torr. Typical evaporation rates on an XTM were 3–5 Å s^{-1}, and the evaporation parameters were adjusted so that the film thickness was near 600 Å. Hf–Ni ribbons were made by melt spinning the arc-melted alloy ingots in Ar gas with a single-roller melt spinner. The purity of Hf was 99.7% and that of Ni was 99.99%. The typical width and the thickness of the ribbons were about 2 mm and 20 μm, respectively.

After warming the thin-film samples to room temperature, they were taken out of the UHV system. The edges of the films were then trimmed to remove the regions of compositional inhomogeneity due to shadowing, and they were mounted in a variable-temperature cryostat for transport measurements. The sample chamber was pumped out and filled with low-pressure He gas to insure that the samples and the thermometer were in thermal equilibrium. The temperature of the sample chamber was controlled to within 30 mK using a Lakeshore cryogenics capacitance temperature controller. A calibrated carbon glass thermometer was used for temperature measurements below 50 K while a calibrated Pt thermometer was used above 50 K. After completion of the transport measurements the composition of the samples was determined by wavelength dispersive spectroscopy using an electron microprobe. The composition of each film was measured at several points to check the sample homogeneity and the variation was within the overall accuracy of the technique, which is 2 at.%. The thickness of the films was measured using a Varian Å-scope. The uncertainty of this technique is about 10%. The values of the thickness were not corrected for the thin oxide layer formed during the exposure of the films to the atmosphere.

The thickness of the ribbons was calculated by measuring the density and the weight of a piece of each sample of known width and length. The amorphous nature and the crystallization temperature of the ribbons were checked using a x-ray diffractometer and a Dupont differential-scanning calorimeter. However, the amorphous nature of the thin films was not checked. Electrical leads were spot welded onto the tabs made by trimming the edges of the ribbons for transport measurements of the ribbons. We were unable to make completely amorphous Hf–Ni ribbons for $0.45 \leqslant x \leqslant 0.55$.

Four-terminal DC resistance measurements were made for both current directions to eliminate thermal EMFs over the temperature range from 1.7 K to 300 K. Three-terminal DC Hall measurements were made in fields of up to 6 T which were provided by a superconducting solenoid. The field was varied in steps of approximately 0.1–0.5 T at each temperature. In order to measure the field-reversed Hall voltage, the sample was mechanically flipped at each field value and the current was reversed at each data point.

3. Results

The resistivities at 4.2 K of Ti–Ni films and Hf–Ni ribbons are shown in figure 1 as a function of Ni concentration, along with that of Ti–Ni ribbons [12, 14] and Zr–Ni ribbons [3] for comparison. The resistivities of the Ti alloys are much higher than those of the Zr and Hf alloys for $0.1 \leqslant x \leqslant 0.6$, merging together at each end. There is an excellent

agreement among the Ti–Ni resistivities from different sources for $x > 0.4$. However, the ribbon samples show a sudden decrease in resistivity for $x < 0.4$, whereas the films show a gradual decrease. The temperature coefficient of resistivity (TCR) at 300 K, which is also shown in the figure, has small negative values characteristic of high-resistivity amorphous alloys. The temperature dependence of the resistivity of Ti–Ni films is shown in figure 2. Both the resistivity and the magnitude of the TCR show a broad maximum around $0.3 \leqslant x \leqslant 0.4$. The hump seen in the TCR near $x = 0.15$ could be due to the variations in samples prepared at different times or a combination of this with the uncertainty in the concentration.

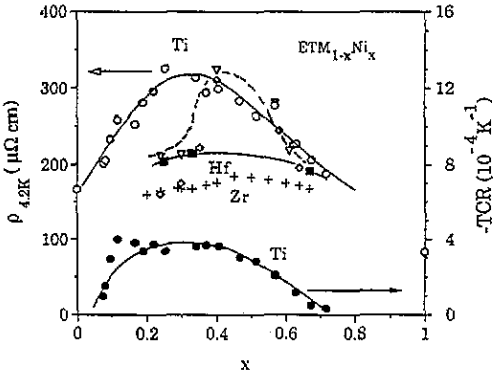

Figure 1. Resistivity ρ at room temperature for Zr–Ni and Hf–Ni, at 4.2 K for Ti–Ni, and temperature coefficient of resistivity TCR at room temperature for Ti–Ni, as a function of Ni composition x for $ETM_{1-x}Ni_x$ alloys: ○, Ti–Ni (this work); ◇, Ti–Ni [12]; ▽, Ti–Ni [14]; +, Zr–Ni [3]; ■, Hf–Ni (this work); ●, TCR (this work). $x = 0$ and $x = 1$ values are for the liquid metals [3]; curves only indicate trends.

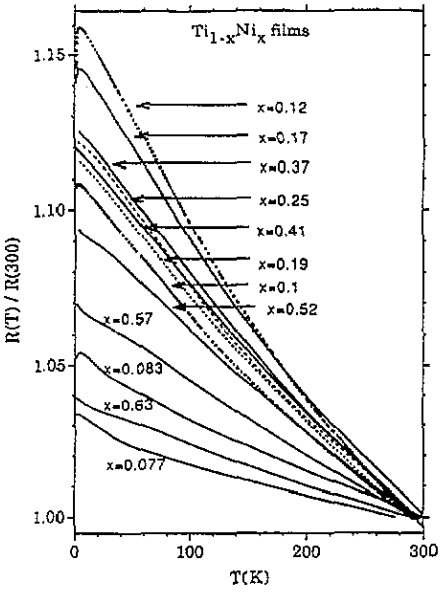

Figure 2. Temperature dependence of the resistivity (normalized to room temperature value) $R(T)/R(300)$, for several $Ti_{1-x}Ni_x$ films.

Hall resistivity as a function of magnetic field was linear for low-x samples, but shows a ferromagnetic behaviour at low fields for higher x values. This behaviour is shown in the inset of figure 3 for $x = 0.72$. The intercept of the linear (high-field) part of the Hall resistivity is shown as a function of temperature in figure 3 for the samples that showed ferromagnetic nature. At the moment we do not understand the small positive intercept seen above 200 K for the $x = 0.63$ sample. The temperature dependence of the Hall coefficient calculated using the high-field data for selected samples is shown in figure 4. R_H has a very small temperature dependence, very similar to that observed for Zr–Ni alloys [9]. The values of the Hall coefficient at 4.2 K for Ti–Ni films are shown in figure 5 along with the room-temperature data on Hf–Ni, Zr–Ni ribbons and films [9, 10] and 77 K data on Ti–Ni ribbons [14] for comparison.

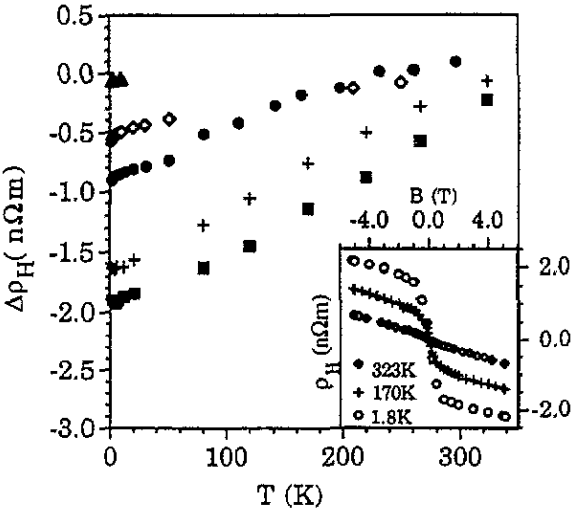

Figure 3. Temperature dependence of the anomalous offset of the Hall resistivity $\Delta\rho_H$ for $Ti_{1-x}Ni_x$ films: ▲, $x = 0.515$; ◊, $x = 0.57$; ●, $x = 0.63$; +, $x = 0.675$; ■, $x = 0.72$. The inset shows ρ_H as a function of field for $x = 0.72$ films at three different temperatures.

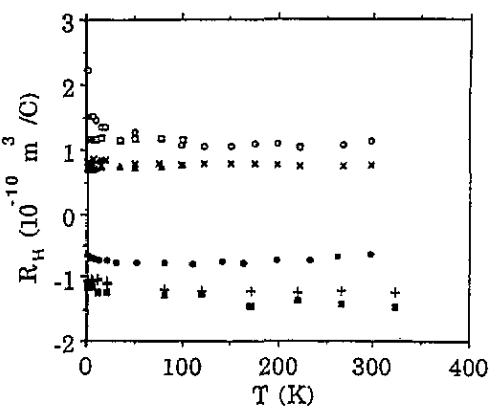

Figure 4. Temperature dependence of the Hall coefficient for selected $Ti_{1-x}Ni_x$ films: ▲, $x = 0.083$; □, $x = 0.165$; ○, $x = 0.254$; ×, $x = 0.34$; ●, $x = 0.63$; +, $x = 0.675$; ■, $x = 0.72$.

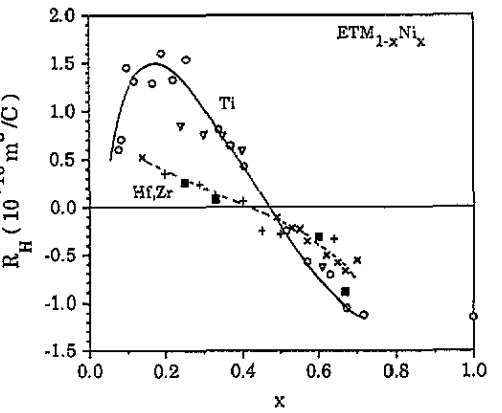

Figure 5. Hall coefficient of $ETM_{1-x}Ni_x$ alloys as a function of composition x: ○, Ti–Ni at 4.2 K (this work); ■, Hf–Ni at 300 K (this work); ▽, Ti–Ni at 77 K ([14]); +, Zr–Ni at 300 K ([10]); ×, Zr–Ni at 300 K [7]; curves indicate trends in the data.

The densities and crystallization temperature for $Hf_{1-x}Ni_x$ ribbons are given in table 1. The DSC curve for the $x = 0.25$ ribbon showed three peaks and the crystallization temperatures for $x = 0.60$ and 0.67 ribbons are beyond the range of our DSC. The $x = 0.5$ alloy indicated crystalline inclusions in the x-ray diffraction measurements.

4. Discussion

We report new resistivity and temperature dependence of resistivity measurements for a

Table 1. Densities and crystallization temperatures of several $Hf_{1-x}Ni_x$ alloys.

x	Density (g cm^{-3})	Crystallization temperature T_x (°C)
0.25	12.50	444 (500, 518)
0.33	12.20	505
(mixed phase) 0.50	11.75	521
0.60	11.39	—
0.67	11.17	—

wide composition range of Ti–Ni alloys. The high resistivities, small negative TCR, smooth variation with composition and the agreement of our data with the few values in the literature are taken as evidence for our samples being amorphous. Nevertheless, since weak localization and electron–electron interaction contributions seem to be important [3, 14], we will postpone further discussions of resistivity and its temperature dependence until magnetoresistance measurements and their analysis are available. Consequently, we will concentrate on the Hall effect measurements.

The two most commonly used approaches for the explanation of the positive Hall coefficients, (1) the s–d hybridization model and (2) the side-jump effect are entirely different mechanisms. It is well known that the s–d hybridization strongly affects the electronic properties. It was proposed [15] that this leads to a S-shaped dispersion curve, hence positive Hall coefficients due to the negative group velocity. Gallagher *et al* [5] reported that the Hall coefficients of Cu-based amorphous alloys (Zr–Cu, Hf–Cu, Ce–Cu, Ti–Cu, Pr–Cu) normalized to free electron values ($R_H/|R_H^0|$), except for Ti–Cu, lie on a single curve as a function of Cu content and discussed this behaviour in terms of an s–d hybridization model. Unfortunately, there is no simple s–d hybridization theory, and very detailed calculations are required for direct comparison of theory with the experiment.

Figure 6 shows the Hall coefficient of Ti–Ni, Zr–Ni and Hf–Ni alloys normalized to the magnitude of the free-electron value calculated assuming that Ti, Zr and Hf atoms contribute two conduction electrons each and that Ni contributes 0.6 electrons. In the case of Ti–Ni films for which measured densities were not available, the density of each alloy was calculated using the bulk densities of Ti and Ni. A prominent feature of the results of figures 5 and 6 is that x_c, the composition at which R_H changes sign, lies between 0.4 and 0.5 for all three alloys in the same column. Thus, x_c does not vary appreciably with ETM row for the IVA column. The values of $R_H/|R_H^0|$ for all three alloys approach the same value near $x < 0.1$ and $x > 0.5$, and R_H approaches the free-electron value as x tends to unity. The Zr and Hf data lie on a single curve, but the Ti alloys exhibit a qualitatively different behaviour. Although the calculated densities may be a few percent different from the actual values, this could not account for the large differences in $R_H/|R_H^0|$. Since Ti, Zr and Hf all have the same number of d electrons, it would not be unreasonable to expect the normalized R_H to follow a universal curve on the basis of the s–d hybridization model. To our knowledge, however, calculations of R_H based on the s–d hybridization model for TM alloys in which both components are dominated by d states are not available for a comparison with the experimental data.

On the other hand, the side-jump mechanism [16] arises due to the asymmetric phase shift introduced in scattering of d electrons in the presence of the spin–orbit interaction. Several authors [4, 7, 11, 17–19] have suggested that this effect may provide an explanation for the positive values of R_H in paramagnetic TM alloys. Trudeau *et al* [11] have expressed the anomalous contribution due to the side-jump effect ΔR_H as

$$\Delta R_H = R_H - R_H^0 = 2e^2\lambda_{so}^{SJ}\chi_v\rho^2/\hbar\mu_0 g_L\mu_B \qquad (1)$$

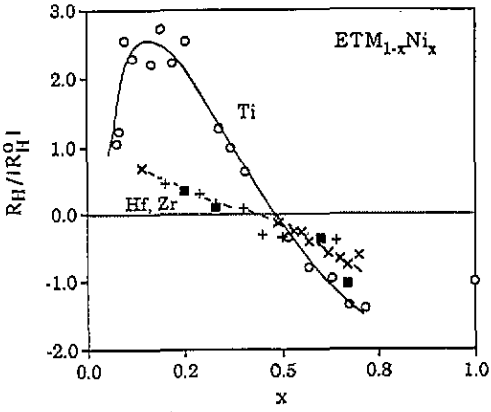

Figure 6. $R_H/|R_H^0|$ as a function of composition for $ETM_{1-x}Ni_x$ alloys: ○, Ti–Ni at 4.2 K (this work); +, Zr–Ni at 300 K [10]; ×, Zr–Ni at 300 K [7]; ■, Hf–Ni at 300 K (this work). The curves indicate trends.

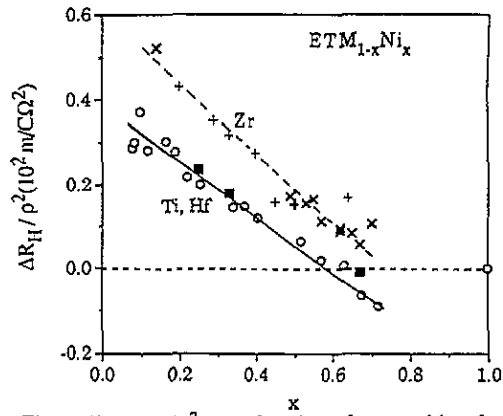

Figure 7. $\Delta R_H/\rho^2$ as a function of composition for $ETM_{1-x}Ni_x$ alloys: ○, Ti–Ni at 4.2 K (this work); ■, Hf–Ni at 300 K (this work); +, Zr–Ni 300 K [10]; ×, Zr–Ni at 300 K [7]. The curves indicate trends.

where R_H is the measured Hall coefficient, R_H^0 is the free-electron contribution, χ_v is the Stoner-enhanced Pauli susceptibility for paramagnetic alloys, g_L is the Lande g factor and μ_B is the Bohr magneton. The crystal-field-enhanced effective spin–orbit interaction parameter is given by

$$\lambda_{so}^{SJ} = \sum_n \frac{|\langle n|\bar{L}|0\rangle|^2}{E_n - E_F} I d^2 A_{so} \tag{2}$$

where the sum is over both filled and unfilled states, I is the overlap integral at the scatterers and A_{so} is the atomic spin–orbit parameter. According to this result the anomalous contribution to the Hall coefficient ΔR_H should vary linearly with $(\chi_v \lambda_{so}^{SJ})\rho^2$.

Naugle, Rhie and coworkers [4, 19] have argued that the side-jump mechanism as described in equations (1) and (2) provides an explanation for the occurrence of a positive Hall coefficient in ETM-based amorphous alloys and, moreover, a viable framework for understanding the composition dependence of R_H for a wide range of Zr-LTM binary and (Zr-LTM)-SM pseudobinary amorphous alloys. The frequently large values of R_H for amorphous Ti-based alloys relative to the Zr-based alloys, e.g. in figure 5 and review articles [3] and [4], is counter-intuitive to the idea that the spin–orbit interaction is responsible, however, since Ti would be expected to have the smaller spin–orbit interaction. In figure 7 $\Delta R_H/\rho^2 = (R_H - R_H^0)/\rho^2$ is plotted as a function of the Ni concentration x for samples from the three alloy series. In terms of the side jump mechanism the ordinate would be proportional to $\lambda_{so}\chi_v$ according to equation (1). A difficulty in establishing the ρ^2 dependence of equation (1) by measurements on a single alloy family is that ρ rarely varies even as much as the 50% change for the Ti–Ni alloys shown in figure 1, and the other quantities are also changing appreciably with composition. The fact that the data for the three different families of alloys lie roughly along similar curves (approximately straight lines over this composition range) appears to substantiate a ρ^2 dependence of the Hall coefficient, thus supporting the arguments for the side-jump contribution. When divided by ρ^2 the data for Ti lie below those for Zr, more in agreement with intuition. Surprisingly, the data for Ti and Hf alloys almost coincide in this figure. The valence susceptibility χ_v has not been determined for either Ti– or Hf–Ni alloys.

We note that Movaghar and Cochrane [20,21] have raised objections to the original derivation [16] of the side-jump contribution. Nevertheless, in their calculations they did find a term [21] that reduces to equations (1) and (2) without having to introduce the idea of a side jump as originally proposed by Berger. We have used the original term 'side-jump' to describe the anomalous term without regard to the controversy regarding its actual origin.

5. Conclusions

Resistivity and Hall-coefficient measurements have been reported for a wide composition range of Ti–Ni alloys and some Hf–Ni alloys. The critical concentration x_c of Ni at which R_H changes sign from positive to negative is around 0.45. Similar behaviour of $\Delta R_H/\rho^2$ for the three (Ti, Zr, Hf) alloys with Ni suggests a ρ^2 dependence of R_H and favours the side-jump effect as the source of the positive contribution to the Hall coefficient although no definitive conclusion can be made without additional experimental data for χ_v and valid calculations of λ_{so}. We have been unable to prepare the anomalous phase of the Hf–Ni alloys at compositions near x_c by melt quenching. The success of cocondensation of amorphous Ti–Ni alloys from the vapour indicates that cocondensation onto liquid-nitrogen-cooled substrates may extend the composition range for formation of amorphous $Hf_{1-x}Ni$ alloys.

Acknowledgments

The authors would like to thank P W Watson and J M Eyhorn for their help in preparing the films and R Guilmette for the electron microprobe analysis. This work was supported by the Robert A Welch Foundation and the National Science Foundation (DMR-89-03135). Two of us gratefully acknowledge a graduate (KR) and an undergraduate (BDH) Robert A Welch Fellowship.

References

[1] Mizutani U 1983 *Prog. Mater. Sci.* **28** 2
[2] Naugle D G 1984 *J. Phys. Chem. Solids* **45** 367
[3] Howson M A and Gallagher B L 1988 *Phys. Rep.* **170** 265
[4] Naugle D G and Rhie K 1993 *Ordering Disorder: Prospect and Retrospect in Condensed Matter Physics (Conf. Proc. Ser. No. 286)* ed V Srivastava, A K Bhatnagar and D G Naugle (New York: American Institute of Physics) pp 58–71
[5] Gallagher B L, Greig D, Howson M A and Croxon A A M 1982 *J. Phys. F: Met. Phys.* **13** 119
[6] v Minnigerode G and Böttjer H G 1985 *Z. Phys.* B **60** 119
[7] Cochrane R W, Destry J and Trudeau M 1983 *Phys. Rev.* B **27** 5955
[8] Ivkov J, Babic E and Jacobs R L 1984 *J. Phys. F: Met. Phys.* **14** L53
[9] Morel R, Huai Y and Cochrane R W 1988 *J. Appl. Phys.* **64** 5462
[10] Trudeau M L, Cochrane R W and Destry 1988 *J. Mater. Sci. Eng.* **99** 187
[11] Trudeau M L, Cochrane R W, Baxter D V, Ström-Olsen J O and Muir W B 1988 *Phys. Rev.* B **37** 4499
[12] Buschow K H J 1983 *J. Phys. F: Met. Phys.* **13** 563
[13] Buschow K H J 1984 *J. Appl. Phys.* **56** 304
[14] Lindqvist P, Kempf A and Fritsch G 1992 *Z. Phys.* B **88** 159
[15] Weir G F, Howson M A, Gallagher B L and Morgan G J 1983 *Phil. Mag.* **47** 136
[16] Berger L 1970 *Phys. Rev.* B **22** 4559
[17] Rhie K, Naugle D G and Bhatnagar A K 1990 *Z. Phys.* B **78** 411
[18] Rhie K and Naugle D G 1990 *Phys. Lett.* **149A** 301

[19] Rhie K, Naugle D G, Beom-Hoan O and Market J T 1993 *Phys. Rev.* B **48** at press
[20] Movaghar B and Cochrane R W 1991 *Phys. Status Solidi* b **166** 311
[21] Movaghar B and Cochrane R Q 1992 *Z. Phys.* B **85** 217